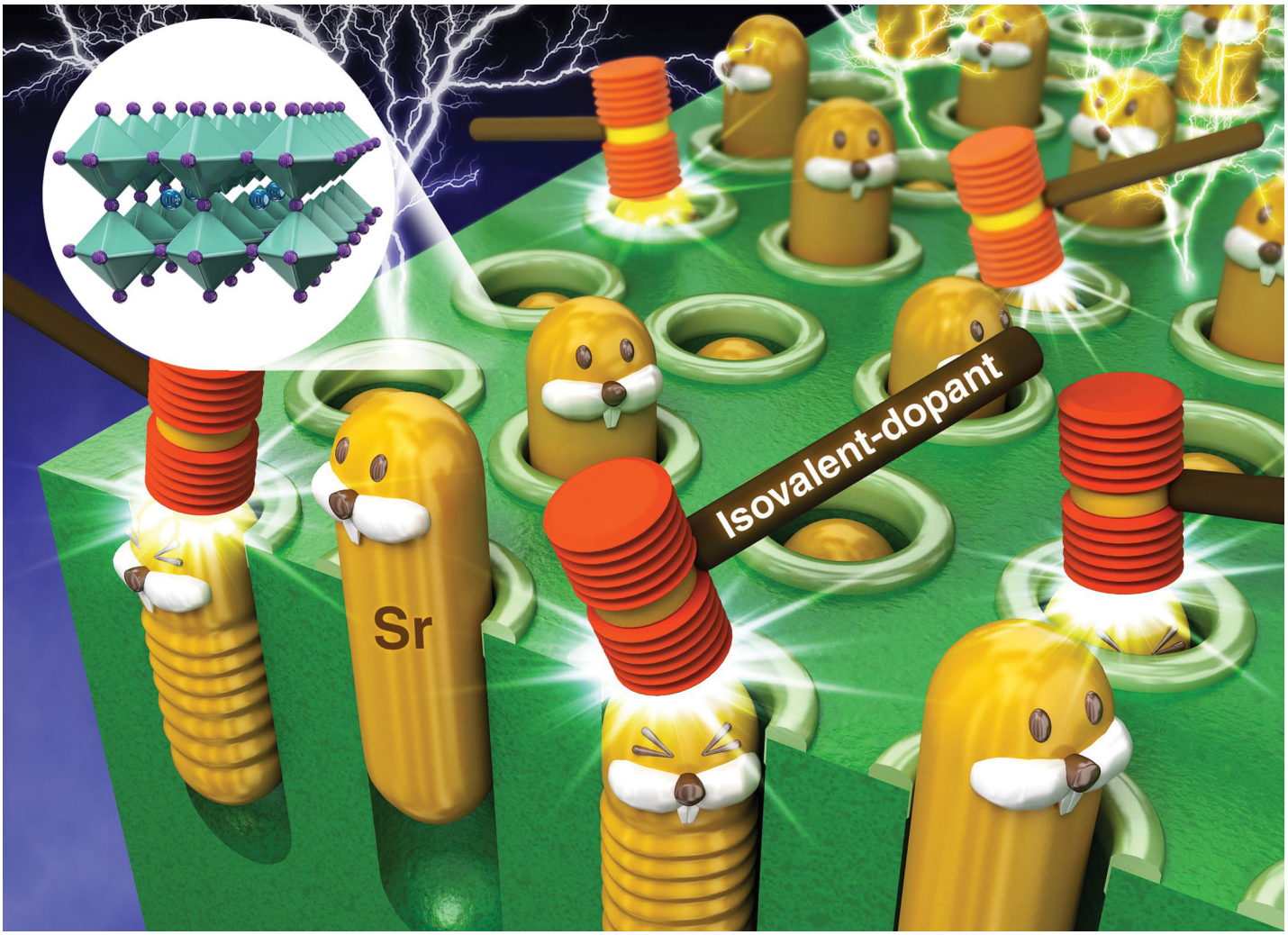

Showcasing research from Prof. WooChul Jung's group at Korea Advanced Institute of Science and Technology and Prof. Jeong Woo Han's group at the University of Seoul, South Korea.

Enhanced oxygen exchange of perovskite oxide surfaces through strain-driven chemical stabilization

The degradation of electrode performance due to the surface chemical instability of perovskite oxides at high operating temperatures is a grand challenge for the development of solid oxide electrochemical cells. In this study, we succeeded in controlling the bond strengths between cations and oxygen ions in a perovskite lattice *via* isovalent doping and thus improving the electrode durability.

As featured in:

See Jeong Woo Han, WooChul Jung *et al.*, *Energy Environ. Sci.*, 2018, **11**, 71.

ROYAL SOCIETY OF CHEMISTRY

rsc.li/ees

Registered charity number: 207890

Energy & Environmental Science

COMMUNICATION

View Article Online
View Journal | View Issue

Check for updates

Cite this: *Energy Environ. Sci.*, 2018, **11**, 71

Received 18th March 2017,
Accepted 13th September 2017

DOI: 10.1039/c7ee00770a

rsc.li/ees

Published on 27 September 2017. Downloaded on 18/01/2018 01:02:48.

Enhanced oxygen exchange of perovskite oxide surfaces through strain-driven chemical stabilization†

Bonjae Koo,‡[a] Hyunguk Kwon,‡[b] YeonJu Kim,[a] Han Gil Seo,[a] Jeong Woo Han*[b] and WooChul Jung*[a]

Surface cation segregation and phase separation, of strontium in particular, have been suggested to be the key reason behind the chemical instability of perovskite oxide surfaces and the corresponding performance degradation of solid oxide electrochemical cell electrodes. However, there is no well-established solution for effectively suppressing Sr-related surface instabilities. Here, we control the degree of Sr-excess at the surface of $SrTi_{0.5}Fe_{0.5}O_{3-\delta}$ thin films, a model mixed conducting perovskite O_2-electrode, through lattice strain, which significantly improves the electrode surface reactivity. Combined theoretical and experimental analyses reveal that Sr cations are intrinsically under a compressive state in the $SrTi_{0.5}Fe_{0.5}O_{3-\delta}$ lattice and that the Sr–O bonds are weakened by the local pressure around the Sr cation, which is the key origin of surface Sr enrichment. Based on these findings, we successfully demonstrate that when a large-sized isovalent dopant is added, Sr-excess can be remarkably alleviated, improving the chemical stability of the resulting perovskite O_2-electrodes.

Broader context

Solid oxide electrochemical cells (SOCs) provide environmentally friendly energy storage/conversion that can store energy in the form of chemical fuels (electrolysis mode) or convert the fuels into electricity (fuel-cell mode) with high efficiency. A key challenge hindering SOC development is severe degradation of the perovskite oxide electrode, primarily due to its chemically unstable surface at high operating temperatures (>600 °C). Here, concurrent studies of lattice strain, surface composition, and surface reactivity of a model perovskite electrode reveal a key driving force of surface chemical inhomogeneity, often called cation segregation. An in-depth understanding of this phenomenon is expected to provide a practical solution for effectively improving the durability of SOC electrodes.

As a carbon-neutral, sustainable future energy technology, solid oxide electrochemical cells (SOCs) have attracted considerable attention because of their high conversion efficiencies, even in the absence of expensive precious metal catalysts.[1,2] SOCs are a general class of electrochemical devices using a solid oxide electrolyte, which include both solid oxide fuel cells (SOFCs) for electricity generation from oxidizing fuels and solid oxide electrolysis cells (SOECs) for the conversion of steam and carbon dioxide into hydrogen and carbon monoxide *via* electricity. A key step in the SOC energy-conversion processes is the oxygen reduction/evolution reaction (ORR/OER) at O_2-electrodes (*i.e.*, the cathode in SOFCs and the anode in SOECs), in which the rapid exchange of oxygen at the electrode surface is critical for facilitating the overall reaction rate.

Perovskite oxides (chemical formula: ABO_3), such as (La,Sr)-(Co,Fe)O_3, (Ba,Sr)(Co,Fe)O_3 and Sr(Fe,Ti,Ni)O_3, have widely been used for SOC O_2-electrode materials given their high electronic and ionic conductivities and favorable catalytic activity for electrode reactions.[3–9] However, the chemical instability of their surfaces, particularly at elevated temperatures (>500 °C), leads to severe degradation of the electrode performance over time. Surface cation segregation and phase separation have recently been suggested as the key reason for the instability of perovskite surfaces. Upon annealing in an oxidizing atmosphere, A-site cation segregation (Sr in particular) near the surface of perovskite oxides has been observed and studied.[5,10–17] Nevertheless, the underlying mechanism for this phenomenon is not completely understood. Therefore, it is unclear how to effectively inhibit the behavior and secure the stability of SOC O_2-electrodes.

It was recently reported that surface Sr enrichment and the resulting formation of SrO_x-like precipitates can be controlled by lattice strain. For example, Yildiz *et al.* observed changes in surface composition under lattice strain in $La_{0.8}Sr_{0.2}CoO_3$ and $La_{0.7}Sr_{0.3}MnO_3$ epitaxial thin films.[18,19] Basu *et al.* reported a similar result in that the Sr concentration increases on the surface of tensile-strained $La_{1-x}Sr_xCo_{0.2}Fe_{0.8}O_3$ films.[20] We have

[a] *Department of Materials Science and Engineering, Korea Advanced Institute of Science and Technology (KAIST), Daejeon, Republic of Korea. E-mail: wcjung@kaist.ac.kr*

[b] *Department of Chemical Engineering, University of Seoul, Seoul, Republic of Korea. E-mail: jwhan@uos.ac.kr*

† Electronic supplementary information (ESI) available: Experimental methods and supplementary data. See DOI: 10.1039/c7ee00770a

‡ These authors contributed equally to this work.

Published on 27 September 2017. Downloaded on 18/01/2018 01:02:48.

also proposed that mechanical strain can be a key factor for surface SrO_x precipitation in $SrTi_{1-x}Fe_xO_3$ thin film electrodes.[21,22] These results elucidate the mechanism to a certain extent, but have yet to provide an ultimate solution to prevent electrode degradation which can be readily applied to real devices.

This study investigates the influence of the Sr–O bond strength in a strained perovskite lattice on surface Sr-excess. Considering dense thin films of $SrTi_{0.5}Fe_{0.5}O_{3-\delta}$ (STF) as a model system, which is representative of a mixed ionic electronic conducting (MIEC) perovskite oxide electrode, we control the lattice strain of STF films by epitaxially growing them onto single-crystal substrates with different lattice parameters, and monitor how the surface composition and oxygen exchange kinetics change accordingly. STF is a model system suitable for this study due to the excellent phase stability and simplicity of its composition. Despite there being a large number of oxygen vacancies, this material system maintains a disordered cubic structure over a wide range of temperatures, gas atmospheres and compositions, except with 100% Fe.[23] Furthermore, Sr in an STF lattice, a neutral constituent and not an aliovalent dopant with an effectively negative charge, can allow us to focus on the elastic effects of strain, neglecting the effects of electrostatic interactions between the cations at the A-site.[16] Here, we found that tensile strain inhibits surface Sr enrichment significantly and enhances the surface oxygen exchange rate, whereas large amounts of excess Sr were observed on the surfaces of compressed films. DFT calculations showed that local compressive states around the Sr atoms in a $SrTiO_3$-type perovskite lattice weakened the Sr–O bond strength, which in turn promoted Sr-excess. We conclusively demonstrated that the compressive strain could be sufficiently alleviated by introducing a large-sized isovalent dopant, suggesting a new strategy for improving the chemical stability of perovskite O_2-electrodes for high-performance SOCs.

First, we fabricated strain-controlled STF thin films by pulsed laser deposition (PLD) on three single-crystal substrates (*i.e.*, $LaAlO_3$(001), $SrTiO_3$(001) and $DyScO_3$(110), which are referred to as LAO, STO and DSO, respectively), and measured their surface compositions and oxygen exchange rates by angle-resolved X-ray photoelectron spectroscopy (AR-XPS) and electrical conductivity relaxation (ECR), respectively. Transmission electron microscopy (TEM) and atomic force microscopy (AFM) confirmed that the epitaxial films with a thickness of 25 nm and smooth surfaces (*i.e.*, surface roughness < 1 nm) were grown (Fig. S1, S2 and Table S1, ESI†). The misfit strain of each film for both in-plane and out-of-plane directions was calculated by high-resolution X-ray diffraction (HR-XRD), as shown in Fig. 1. The resulting films have larger relaxed unit cell volumes than those in bulk samples, likely due to oxygen deficiency in the PLD films.[24] Accordingly, the values of the relaxed lattice parameter ($\hat{a}$) of each film, as a reference, were calculated by combining the interplanar distance of the (002) and (110) peaks with a Poisson ratio of 0.232,[25] and the levels of both in-plane and out-of-plane strain were then defined by their deviations from $\hat{a}$, as reported by Shao-Horn *et al.*[26] The STF thin films on LAO and STO substrates are compressed in-plane and dilated in the direction normal to the film surface (*i.e.*, in-plane strain (ε_{aa}) of -3.04% and -1.48%, respectively). On the other hand, the film on DSO shows tensile strain along the in-plane direction (*i.e.*, ε_{aa} of $+0.61\%$) (see Table 1). This is also supported by the average interatomic distance of the three films measured by scanning transmission electron microscopy (STEM) (Fig. S1, ESI†). The absolute misfit strain of the STF films is remarkably high. For example, the in-plane strain of -3.04% in the film on LAO roughly corresponds to a mechanical stress of ~ 7.13 GPa, given a biaxial modulus of 233 GPa of $SrTiO_3$.[27]

The chemical composition of each film was analyzed at different depths from the surface *via* AR-XPS, focusing on the effects of lattice strain on surface Sr enrichment. Fig. 2 presents the photoelectron spectra of each constituent cation in STF films at emission angles of 0° and 75°. Because a higher emission angle is more surface sensitive (*e.g.*, corresponding to average depths of

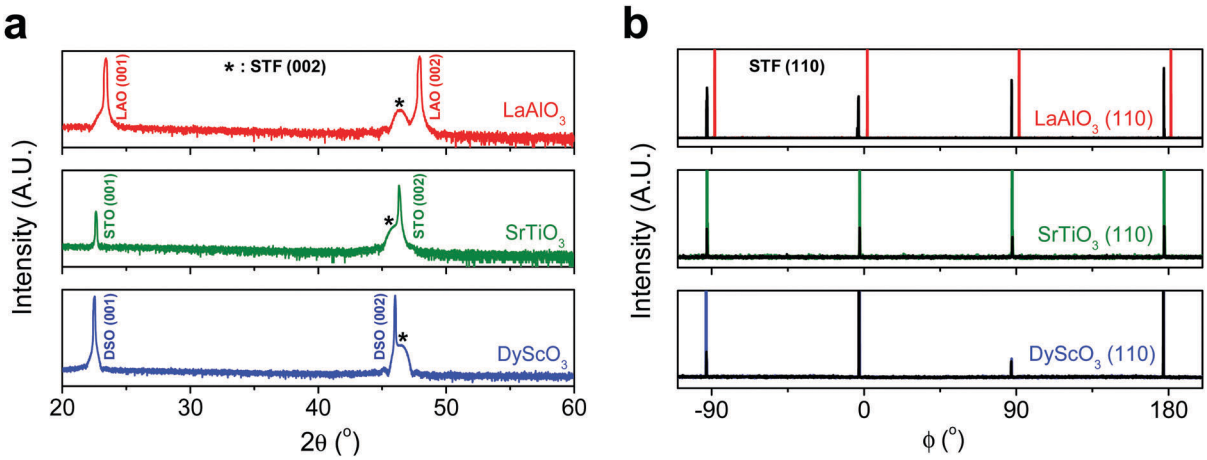

Fig. 1 High-resolution X-ray diffraction (HR-XRD) results of epitaxial $SrTi_{0.5}Fe_{0.5}O_{3-\delta}$ (STF) thin films on single-crystal substrates. (a) Out-of-plane diffraction patterns (2θ scan) of the (001)-oriented epitaxial STF thin films on $LaAlO_3$(001), $SrTiO_3$(001) and $DyScO_3$(110) substrates. (b) In-plane diffraction patterns (φ scan) of the (001)-oriented epitaxial STF thin films on each substrate. Each φ scan was collected for the (110) peak after tilting the sample by 45°.

 This journal is © The Royal Society of Chemistry 2018

Published on 27 September 2017. Downloaded on 18/01/2018 01:02:48.

Table 1 Calculated misfit strain of $SrTi_{0.5}Fe_{0.5}O_{3-\delta}$ (STF) thin films. The strained and relaxed lattice parameters of epitaxial STF thin films were collected from HR-XRD data. The strained in-plane and out-of-plane lattice parameters of the STF films were calculated by combining the interplanar distance of the (002) and (110) peaks

Substrate	Strained in-plane lattice parameter a (Å)	Strained out-of-plane lattice parameter c (Å)	Relaxed film lattice parameter[a] $\hat{a}$ (Å)	In-plane strain (%) $\varepsilon_{aa} = \frac{(a-\hat{a})}{\hat{a}}$	Out-of-plane strain (%) $\varepsilon_{cc} = \frac{(c-\hat{a})}{\hat{a}}$
$LaAlO_3$ (3.790 Å)	3.800	3.992	3.920 ± 0.006	−3.04 ± 0.14	1.86 ± 0.24
$SrTiO_3$ (3.905 Å)	3.851	3.944	3.909 ± 0.006	−1.48 ± 0.15	0.89 ± 0.22
$DyScO_3$ (3.948 Å)	3.942	3.904	3.918 ± 0.006	0.61 ± 0.15	−0.36 ± 0.22

[a] $\hat{a}$ was calculated using $\frac{\Delta c}{\hat{c}} = \frac{-2V}{1-V}\frac{\Delta a}{\hat{a}}$, assuming $\hat{a} = \hat{c}$ and $\nu = 0.232$[25] for STF.

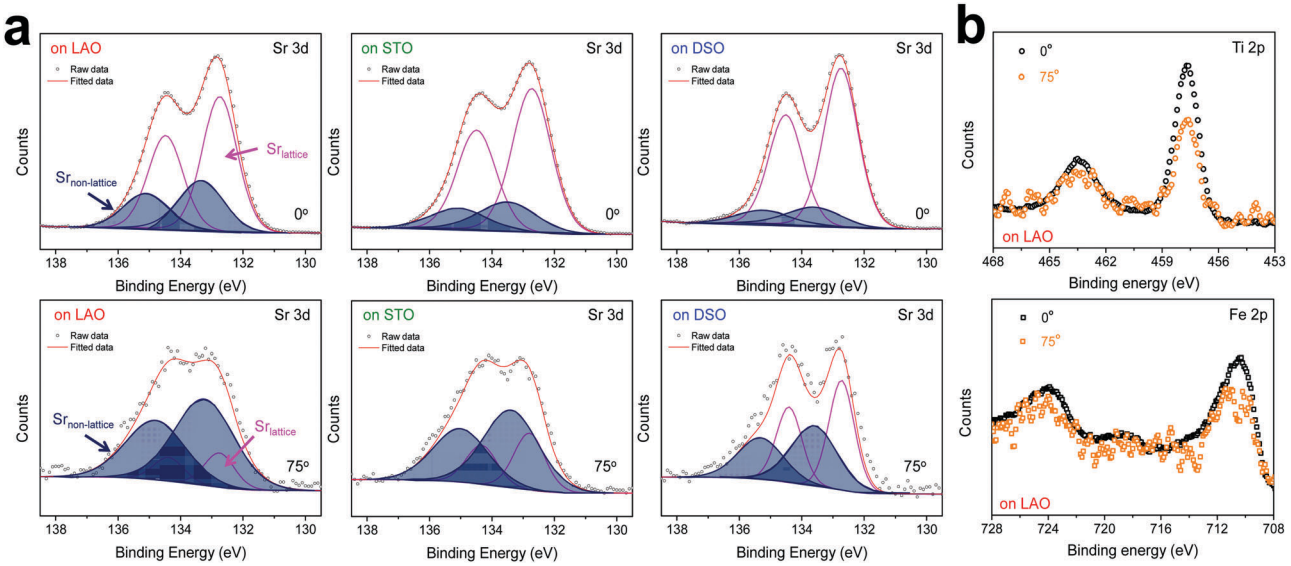

Fig. 2 Angle-resolved X-ray photoelectron spectroscopy (AR-XPS) results of each constituent cation in strained-$SrTi_{0.5}Fe_{0.5}O_{3-\delta}$ (STF) surfaces. (a) Sr 3d spectra of epitaxial STF thin films on single-crystal $LaAlO_3$ (LAO), $SrTiO_3$ (STO) and $DyScO_3$ (DSO) substrates at emission angles of 0° and 75°. (b) Ti and Fe 2p spectra of epitaxial STF thin films on the LAO substrate at emission angles of 0° and 75°.

~10 nm and ~2.5 nm for 0° and 75°, respectively), it is clear that the Sr 3d peak is markedly different at the surface (=75°) compared to its signature from the bulk (=0°) of the material (Fig. 2a). On the other hand, in contrast to the Sr 3d peak, the Fe and Ti 2p spectra remain largely the same, regardless of the depth from the surface, as shown in Fig. 2b. In fact, the Sr 3d spectra were fitted well using two sets of spin–orbit doublets with an energy separation of ~1.8 eV and an area ratio of 1.5. The main Sr 3d doublet corresponds to Sr in the bulk lattice, whereas the other doublet with the higher binding energy originates from the surface Sr species.[10,11] The surface Sr peaks are dominant for a compressive strained film. In contrast, the main bulk peaks prevail for the film stretched in-plane.

For more quantitative analysis, the relative Sr enrichment with respect to the B-site cation content was calculated by fitting the XPS spectra of each constituent cation measured at different emission angles. To eliminate technical difficulties in the XPS analysis, I_0([Sr/(Ti + Fe)]0°) and I_x([Sr/(Ti + Fe)]x°) were used to refer to the ratio of the A-site cation content to the B-site cation content measured at detection angles of 0° (more bulk sensitive) and X° (more surface sensitive as X° increases), respectively. The I_x/I_0 ratio was then evaluated to represent the relative Sr surface enrichment. As shown in Fig. 3a, the relative Sr intensity (I_x/I_0) increases sharply with increasing emission angle, particularly for the compressed film on LAO, confirming the appreciable degree of Sr-excess at the surface of the STF thin film. On the other hand, the Sr intensity decreases with decreasing compressive strain. As a result, the in-plane stretched film on DSO shows a negligible degree of Sr-excess at the surface. In contrast, no surface enrichment in the relative Fe content, which is defined by I_x/I_0([Fe/(Ti + Fe)x°]/[Fe/(Ti + Fe)0°]) at various emission angles, is found, confirming that the surface chemical inhomogeneity results mainly from the Sr redistribution, not Fe or Ti (Fig. S3, ESI†). Note that the bulk composition of STF films was also analyzed by inductively coupled plasma mass spectroscopy (ICP-MS), showing good agreement with that in the target materials (see Table S2, ESI†).

Fig. 3b presents the relaxation profiles of STF films, showing the transient behavior of the conductivity with a step change in the pO_2 of the surrounding gas. Because the thickness of the STF films is below the critical thickness,[28] the relaxation profile reflects the kinetics of the surface exchange reaction, rather

Published on 27 September 2017. Downloaded on 18/01/2018 01:02:48.

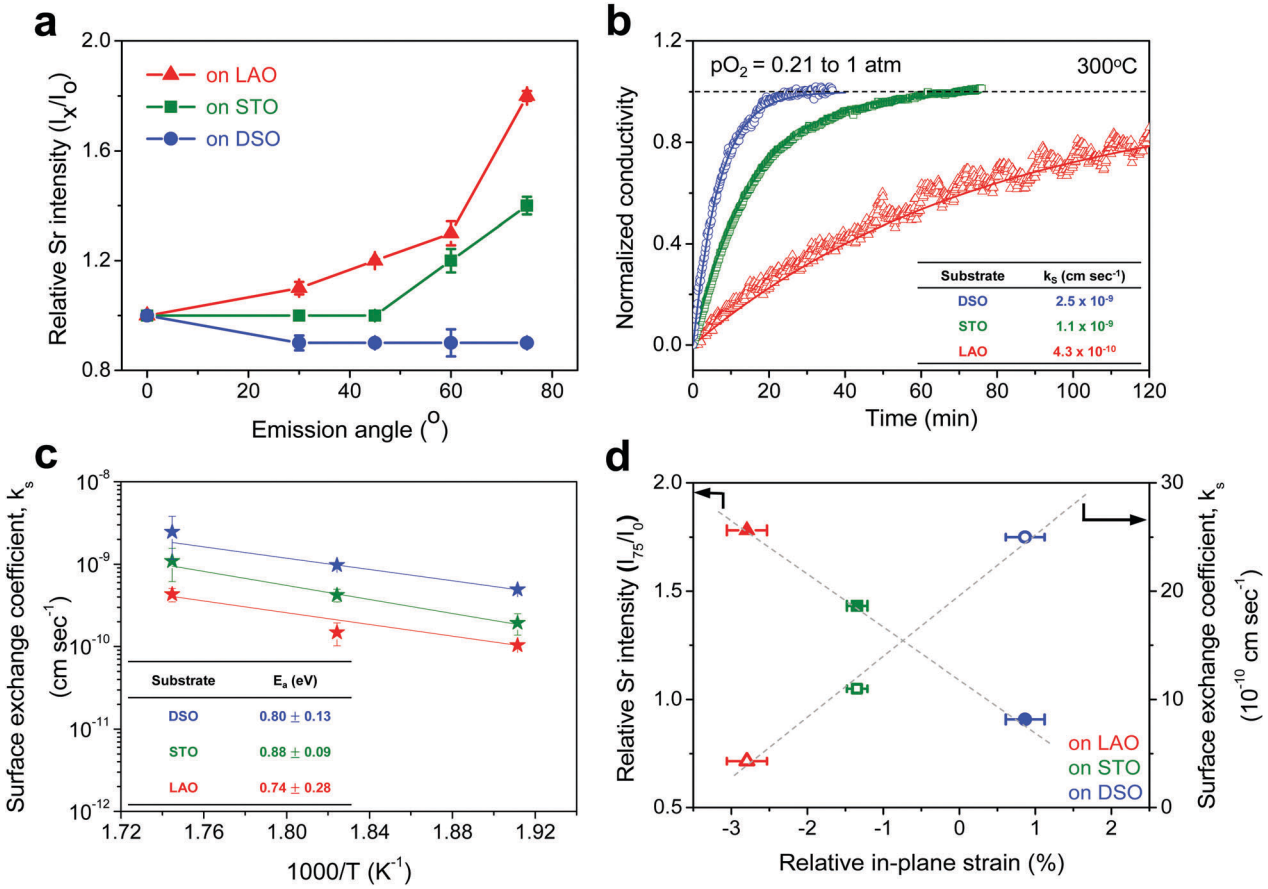

Fig. 3 Surface composition and oxygen exchange kinetics of strained $SrTi_{0.5}Fe_{0.5}O_{3-\delta}$ (STF) thin films. (a) The relative Sr intensity of epitaxial STF thin films on single-crystal $LaAlO_3$ (LAO), $SrTiO_3$ (STO) and $DyScO_3$ (DSO) substrates with varying emission angles (X) from bulk (θ = 0°) to surface (θ = 75°). (b) The normalized conductivity of epitaxial STF thin films on LAO, STO and DSO substrates at 300 °C with switching pO_2 from 1 atm to 0.21 atm. (c) Arrhenius plot of the chemical exchange coefficients (k_s) and the activation energy (E_a) of epitaxial STF thin films on LAO, STO and DSO. (d) Comparison of the relative Sr enrichment and (d) the surface oxygen exchange coefficient (k_s) of epitaxial STF thin films with the degree of induced in-plane strain.

than the bulk diffusion of oxygen. Therefore, the surface oxygen exchange coefficient (k_s) can be calculated using eqn (1) as follows:

$$\frac{\sigma(t)-\sigma(0)}{\sigma(\infty)-\sigma(0)} = 1-\exp\left(-\frac{k_s}{a}t\right) \quad (1)$$

where $\sigma(t)$ and a represent the electrical conductivity at time t and the thickness of the STF film, respectively. Interestingly, the surface reaction rate increases as the film is stretched along the in-plane direction. The k_s value of the film grown on DSO increases by a factor of 6 compared to that on LAO. Similar trends were also observed at different temperatures, and all samples had similar values of activation energy (Fig. 3c). These results show that the ORR/OER activities of a perovskite O_2-electrode can be improved by controlling the lattice strain. Note that the k_s values in this study are smaller compared to those of the bulk sample reported in the literature, which is expected to come from the presence of grain boundaries (Fig. S4, ESI†).

Overall, more tensile strain tends to decrease the levels of Sr-excess and simultaneously enhance k_s (Fig. 3d). Previously, we observed a significant reduction in the area-specific resistance (ASR) of the STF thin film electrodes by chemically etching the Sr-enriched layer, showing that the SrO_x-related species at the STF surfaces serves as a passivation barrier for oxygen exchange.[21,22] Considering these results, the inhibited Sr enrichment by tensile strain is thought to enhance the surface exchange kinetics. Two factors need to be mentioned here. First, this observation is direct evidence supporting the hypothesis we have proposed in previous studies; mechanical strain is a relevant driving force for Sr-rich phases at the STF surfaces.[21,22] The atomistic scale mechanism for strain-driven Sr-excess will be discussed in greater detail below. Second, these results suggest that perovskite surfaces can be stabilized chemically by strain-engineering. Lattice strain influences many material properties, such as electrical conductivity, electronic structure, and defect concentration.[29–31] Several studies have recently reported the strain-driven changes in chemical composition or the oxygen exchange of perovskite surfaces.[18–20,26,32,33] For example, Fleig *et al.* reported that the tensile strain accelerated the tracer surface exchange coefficients in (La,Sr)CoO_3 thin films.[32] Shao-Horn *et al.* showed that the tensile-strained $LaCoO_3$ electrode exhibited a decrease in charge transfer resistance compared to the compressive one.[33] Yildiz *et al.* examined the effects of lattice strain

 This journal is © The Royal Society of Chemistry 2018

Published on 27 September 2017. Downloaded on 18/01/2018 01:02:48.

on the surface electronic and chemical states of $La_{0.8}Sr_{0.2}CoO_3$ and $La_{0.7}Sr_{0.3}MnO_3$ thin films.[18,19] To the best of the authors' knowledge, however, there have been no concurrent studies on the lattice strain, surface chemical composition, and surface reactivity of a mixed conducting perovskite oxide.

From the point of view of defect chemistry, Sr enrichment and the resulting formation of SrO at the perovskite oxide surfaces can be understood as the result of partial Schottky defect formation reaction. In order to form SrO on the surface, Sr and O in the oxide lattice must be pulled out one by one to the surface, as shown in eqn (2).

$$Sr_{Sr}^{\times} + O_O^{\times} = \left(Sr_{surf}^{\bullet\bullet} + O_{surf}''\right) + V_{Sr}'' + V_O^{\bullet\bullet} \qquad (2)$$

Here, we calculated the partial Schottky formation energy ($E_{Schottky}$) which is the energy required for this process as a function of lattice strain through DFT calculations. Fig. 4a shows that $E_{Schottky}$ increases with increasing biaxial strain in the tensile direction, indicating that it is more difficult to form a SrO species on a stretched lattice. Thus, it was validated that the experimental results in Fig. 3a can be explained through thermodynamic aspects.

To elucidate the origin of the surface Sr-excess, we additionally carried out DFT calculations on two elemental thermodynamic steps: "the removal of Sr from the crystal lattice" and "the formation of a product phase on the surface," as explained by Feng *et al.*[34] First, the stability of the Sr atom according to biaxial strain was investigated by calculating the vacancy formation energy of Sr ($E_{Sr,vac}$). Here, we used STO bulk to emphasize that a driving force of Sr enrichment would be generally applied to the various types of STO-based perovskites. In addition, by using the STO bulk model instead of STF, the complexity of configurations at the B-site caused by Fe doping can be removed. Indeed, it turns out that our main reasoning can also be applied to STF as well as STO (Fig. S5, ESI†). Fig. 4b shows that $E_{Sr,vac}$ decreases under compressive strain due to the weakened Sr–O bond strength, which explains the experimentally observed Sr enrichment at the compressive strained surface in Fig. 3d. Meanwhile, an interesting tendency of $E_{Sr,vac}$ was found in the range of tensile strain. $E_{Sr,vac}$ continues to increase rather than decrease with increasing tensile strain. To investigate this behavior in detail, the bond length between the nearest Sr and O was calculated according to the biaxial strain (Fig. S6, ESI†). When a cubic STO perovskite is biaxially strained, the equivalent twelve Sr–O bonds are differentiated into two types (bond A and bond B in Fig. S6a, ESI†). Although all Sr–O bond lengths are no longer identical under the applied strain, the two types of bond lengths increase nonetheless when applying biaxial tensile strain (Fig. S6b, ESI†). In the strain-free equilibrium state, the Sr–O bond length is shorter than the optimal Sr–O bond length in the most stable state within the bulk lattice where $E_{Sr,vac}$ would be the highest. Owing to the shorter bond length in the strain-free state compared to that in the tensile-strained state, expansion of perovskite oxide increases $E_{Sr,vac}$ (at least up to the tensile strain of ~1%) while making the Sr atoms more stable. This indicates that Sr atoms are intrinsically in a compressive state in the STO bulk lattice. Accordingly, we concluded that the thermodynamic instability of Sr in the bulk lattice as identified in this calculation can cause the strain-driven enrichment phenomenon, thus explaining our experimental observations.

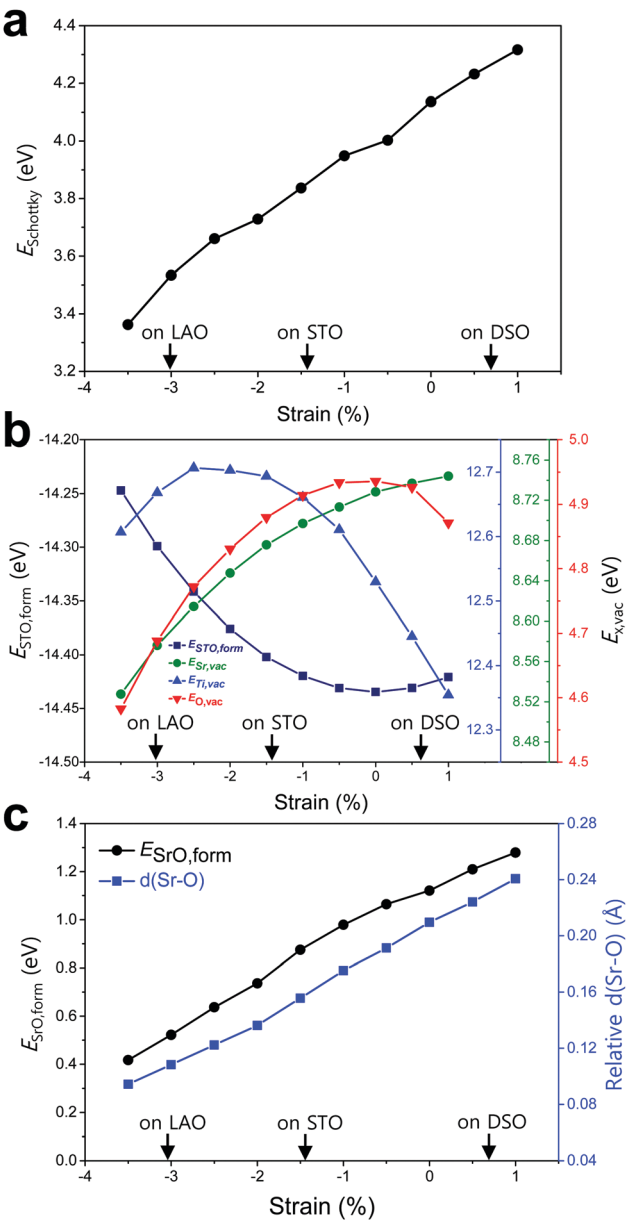

Fig. 4 Strain-dependent energetic states of $SrTiO_3$ (STO) and $SrTi_{0.5}Fe_{0.5}O_3$ (STF) perovskites. (a) Response of $E_{Schottky}$ upon the applied biaxial strain in the STF surface. (b) $E_{STO,form}$ and $E_{X,vac}$ (X = Ti, O, and Sr) in bulk STO with increasing biaxial strain. (c) $E_{SrO,form}$ and d(Sr–O) in an SrO monolayer on the STF surface relative to that in the bulk SrO as a function of the applied biaxial strain.

To further understand the structural characteristics of STO perovskite and confirm the validity of our argument that Sr atoms are instrinsically under a local compressive state, we also calculated the formation energy of STO perovskite ($E_{STO,form}$) and the vacancy formation energies of its constituent elements ($E_{Ti,vac}$ and $E_{O,vac}$). As can be seen in Fig. 4b, $E_{STO,form}$ always increased once the STO perovskite deviated from the zero strain state, due to the weakened bond strengths (Sr–O and/or Ti–O)

Published on 27 September 2017. Downloaded on 18/01/2018 01:02:48.

within the STO perovskite. Since oxygen is bonded with both A-site cations (Sr) and B-site cations (Ti), the dependence of $E_{O,vac}$ on the strain is similar to that of $E_{STO,form}$, both of which have a critical point at zero strain but with the opposite sign of the quadratic curve. On the other hand, $E_{Sr,vac}$ and $E_{Ti,vac}$ show apparently different behaviors compared with $E_{O,vac}$ (Fig. 4b). This reveals that in unstrained STO perovskite, the large Sr atom is under a local compressive state whereas the small Ti atom is under a local tensile state. Although Sr–O and Ti–O may not be in the most stable state individually, they are in an optimal balance at zero strain, thereby stabilizing the overall STO perovskite.

Next, the tendency to form the Sr-rich secondary phase on the surface was also evaluated. Since a SrO_x-like insulating phase has been detected experimentally through previous *in situ* STM/STS analysis and is proposed as one of the major product phases formed by Sr-excess,[21,22] the formation energy of an SrO monolayer on the perovskite surface ($E_{SrO,form}$) was calculated in this work (Fig. S7, ESI†). Fig. 4c shows that the SrO monolayer is more difficult to form on the STF surface with increasing biaxial strain, which is in good agreement with both the experimental and computational observations in Fig. 3d and 4a, respectively. To analyse this result, the Sr–O distances between the bulk SrO with space group $Fm\bar{3}m$ and the SrO monolayer formed on the surface were compared. The details for measuring the distances are described in Fig. S8 (ESI†). As shown in Fig. 4c, the average Sr–O distance of the SrO monolayer is longer than that of the bulk SrO, suggesting that the SrO monolayer formed on the STF surface is somewhat stretched. Therefore, a high $E_{SrO,form}$ is observed at the tensile-strained surface to retain its original bulk structure on the STF surface. As a result, the unfavorable SrO formation would have a synergetic effect to lower the Sr enrichment at tensile-strained surfaces in combination with reduced Sr accumulation.

Based on the discussion so far, it was found that surface Sr-excess can be suppressed by intentionally adjusting the bond strength (or length) between Sr and O in a perovskite lattice. Because it is practically impossible to apply direct pressure to the electrodes in operation, an attempt was made to replace the B-site cation with isovalent cations with different sizes, which may relax the compressive strain within the lattice. To explore the appropriate candidate of the dopant cation, the bond length between Sr and O in a bulk $Sr(Ti_{0.25}M_{0.25}Fe_{0.50})O_3$ perovskite (M = transition metal with a formal charge of 4+ and a coordination number of 6) was calculated. Fig. 5a shows the greater increase in the Sr–O bond length by replacing Ti with a larger cation, such as Hf and Zr, and the strength is thus reinforced. Subsequent AR-XPS analysis confirmed that Hf and Zr doping actually suppresses Sr enrichment on the surface. As shown in Fig. 5b, the Sr relative intensity with the emission angle confirmed that the Sr intensity in Hf- and Zr-doped STF films remains constant and unchanged, even if it is near the surface. Considering that this experiment was carried out using thick polycrystalline thin films with little lattice strain applied through the substrate, it is clear that isovalent B-site doping is a useful method for preventing surface cation segregation, and

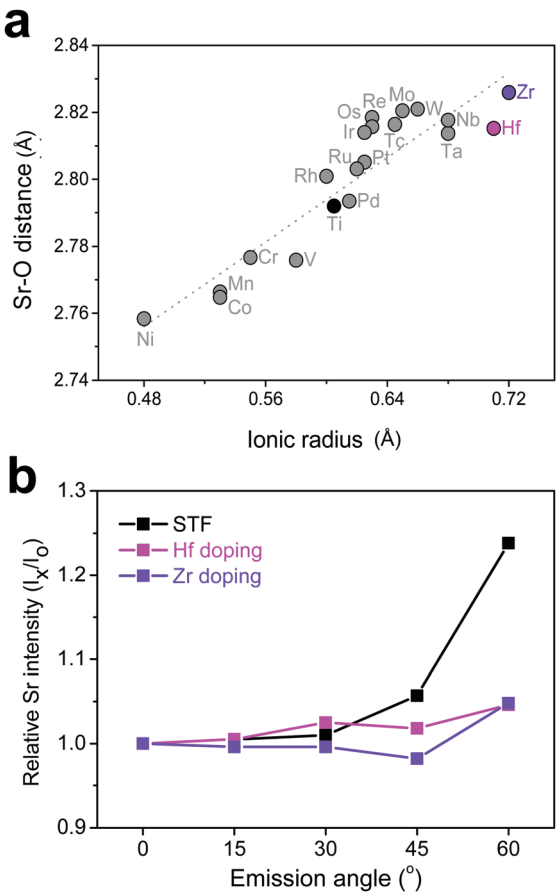

Fig. 5 Isovalent doping effect in Sr enrichment of $SrTi_{0.5}Fe_{0.5}O_{3-\delta}$ (STF). (a) DFT-calculated d(Sr–O) for a wide range of transition metal doped $Sr(Ti_{0.25}M_{0.25}Fe_{0.50})O_3$ perovskites. (b) The relative Sr intensity of polycrystalline STF thin films with Hf and Zr doping with varying emission angles (X) from bulk (θ = 0°) to surface (θ = 60°). Note that a small amount of dopant (2 wt%) was used to prevent significant changes in the properties of the host material and to prevent the Sr–O bond from stretching beyond the predicted optimal length.

this method can be easily applicable to real SOC O_2-electrodes. Recently, Yildiz *et al.* have shown that surface modification with less reducible cations, such as Hf and Zr, can improve the surface chemical and electrochemical stability of $La_{0.8}Sr_{0.2}CoO_3$.[35] They explained that these cations lower the concentration of surface oxygen vacancies that are positively charged and reduce the electrostatic attraction of negatively charged Sr dopants (Sr_{La}') towards the surface. In this study, it is believed that the importance of electrostatic interaction is much weaker in comparison with their case because Sr itself, which is a host rather than an isovalent dopant, is enriched. Therefore, we think that this study proposes a new directional approach that explains a similar surface cation segregation phenomenon in terms of elastic interaction: the local coordinate states around the Sr cation determine the surface stability of Sr-containing perovskite oxides.

This study investigated the lattice strain-driven changes in the surface chemical composition and oxygen exchange kinetics of epitaxial thin films of $SrTi_{0.5}Fe_{0.5}O_{3-\delta}$, as a representative

 This journal is © The Royal Society of Chemistry 2018

Published on 27 September 2017. Downloaded on 18/01/2018 01:02:48.

mixed conducting perovskite O_2-electrode, focusing on surface Sr-excess. The tensile strain in the in-plane direction considerably inhibits enrichment and facilitates the surface reaction rate. DFT calculations showed that the relatively weak bond strength induced by the compressed Sr–O bond in the perovskite lattice drives the increased surface Sr component. Based on these observations, we conclude that the extent of deviation from the optimal A–O bond strength in the most stable state of the A-site cation is the main driving force for surface segregation in ABO_3-type perovskite oxides. Consequently, we offer isovalent doping as an effective way to establish the chemical stability of perovskite oxide surfaces, thereby enhancing the electrode performance in solid oxide electrochemical cells.

Conflicts of interest

There are no conflicts to declare.

Acknowledgements

This study was supported by the Samsung Research Funding Center for Future Technology (G01150336). The authors also acknowledge S.-S. Ha and D. Y. Noh of Gwangju Institute of Science and technology (GIST) for their assistance with XRD analysis.

Notes and references

1 C. Graves, S. D. Ebbesen, S. H. Jensen, S. B. Simonsen and M. B. Mogensen, *Nat. Mater.*, 2015, **14**, 239–244.
2 J. T. S. Irvine, D. Neagu, M. C. Verbraeken, C. Chatzichristodoulou, C. Graves and M. B. Mogensen, *Nat. Energy*, 2016, **1**, 1–13.
3 Y. Ohno, S. Nagata and H. Sato, *Solid State Ionics*, 1981, **3–4**, 439–442.
4 W. Jung and H. L. Tuller, *Adv. Energy Mater.*, 2011, **1**, 1184–1191.
5 G. M. Rupp, T. Téllez, J. Druce, A. Limbeck, T. Ishihara, J. Kilner and J. Fleig, *J. Mater. Chem. A*, 2015, **3**, 22759–22769.
6 E. P. Murray, M. J. Sever and S. A. Barnett, *Solid State Ionics*, 2002, **148**, 27–34.
7 Z. Shao and S. M. Haile, *Nature*, 2004, **431**, 170–173.
8 Y. Chen, W. Zhou, D. Ding, M. Liu, F. Ciucci, M. Tade and Z. Shao, *Adv. Energy Mater.*, 2015, **5**, 1500537.
9 G. Yang, W. Zhou, M. Liu and Z. Shao, *ACS Appl. Mater. Interfaces*, 2016, **8**, 35308–35314.
10 Z. Cai, M. Kubicek, J. Fleig and B. Yildiz, *Chem. Mater.*, 2012, **24**, 1116–1127.
11 E. J. Crumlin, E. Mutoro, Z. Liu, M. E. Grass, M. D. Biegalski, Y.-L. Lee, D. Morgan, H. M. Christen, H. Bluhm and Y. Shao-Horn, *Energy Environ. Sci.*, 2012, **5**, 6081–6088.
12 J. Druce, T. Ishihara and J. A. Kilner, *Solid State Ionics*, 2014, **262**, 893–896.
13 M. Kubicek, A. Limbeck, T. Frömling, H. Hutter and J. Fleig, *J. Electrochem. Soc.*, 2011, **158**(6), B727–B734.
14 H. Wang, K. J. Yakal-Kremski, T. Yeh, G. M. Rupp, A. Limbeck, J. Fleig and S. A. Barnett, *J. Electrochem. Soc.*, 2016, **163**(6), F581–F585.
15 A.-K. Huber, M. Falk, M. Rohnke, B. Luerßen, L. Gregoratti, M. Amati and J. Janek, *Phys. Chem. Chem. Phys.*, 2012, **14**, 751–758.
16 W. Lee, J. W. Han, Y. Chen, Z. Cai and B. Yildiz, *J. Am. Chem. Soc.*, 2013, **135**, 7909–7925.
17 H. Kwon, W. Lee and J. W. Han, *RSC Adv.*, 2016, **6**, 69782–69789.
18 Z. Cai, Y. Kuru, J. W. Han, Y. Chen and B. Yildiz, *J. Am. Chem. Soc.*, 2011, **133**, 17696–17704.
19 H. Jalili, J. W. Han, Y. Kuru, Z. Cai and B. Yildiz, *J. Phys. Chem. Lett.*, 2011, **2**, 801–807.
20 Y. Yu, K. F. Ludwig, J. C. Woicik, S. Gopalan, U. B. Pal, T. C. Kaspar and S. N. Basu, *ACS Appl. Mater. Interfaces*, 2016, **8**, 26704–26711.
21 W. Jung and H. L. Tuller, *Energy Environ. Sci.*, 2012, **5**, 5370–5378.
22 Y. Chen, W. Jung, Z. Cai, J. J. Kim, H. L. Tuller and B. Yildiz, *Energy Environ. Sci.*, 2012, **5**, 7979–7988.
23 A. Rothschild, W. Menesklou, H. L. Tuller and E. Ivers-Tiffée, *Chem. Mater.*, 2006, **18**, 3651–3659.
24 Y. Davila, A. Petitmangin, C. Hebert, J. Perriere and W. Seiler, *Appl. Surf. Sci.*, 2011, **257**, 5354–5357.
25 H. Ledbetter, M. Lei and S. Kim, *Phase Transitions*, 1990, **23**, 61–70.
26 G. Jose la O', S.-J. Ahn, E. Crumlin, Y. Orikasa, M. D. Biegalski, H. M. Christen and Y. Shao-Horn, *Angew. Chem., Int. Ed.*, 2010, **49**, 5344–5347.
27 S. Piskunov, E. Heifets, R. I. Eglitis and G. Borstel, *Comput. Mater. Sci.*, 2004, **29**, 165–178.
28 R. Merkel and J. Maier, *Angew. Chem., Int. Ed.*, 2008, **47**, 3874–3894.
29 C. Solís, M. D. Rossell, G. Garcia, G. Van Tendeloo and J. Santiso, *Adv. Funct. Mater.*, 2008, **18**, 785–793.
30 A. D. Rata, A. Herklotz, K. Nenkov, L. Schultz and K. Dörr, *Phys. Rev. Lett.*, 2008, **100**, 076401.
31 A. Kushima, S. Yip and B. Yildiz, *Phys. Rev. B: Condens. Matter Mater. Phys.*, 2010, **82**, 115435.
32 M. Kubicek, Z. Cai, W. Ma, B. Yildiz, H. Hutter and J. Fleig, *ACS Nano*, 2013, **7**(4), 3276–3286.
33 K. A. Stoerzinger, W. S. Choi, H. Jeen, H. N. Lee and Y. Shao-Horn, *J. Phys. Chem. Lett.*, 2015, **6**, 487–492.
34 Z. Feng, W. T. Hong, D. D. Fong, Y.-L. Lee, Y. Yacoby, D. Morgan and Y. Shao-Horn, *Acc. Chem. Res.*, 2016, **49**, 966–973.
35 N. Tsvetkov, Q. Lu, L. Sun, E. J. Crumlin and B. Yildiz, *Nat. Mater.*, 2016, **15**, 1010–1016.